Human Reproduction, Vol.35, No.1, pp. 44–57, 2020
Advance Access Publication on January 8, 2020 doi:10.1093/humrep/dez247

human reproduction

ORIGINAL ARTICLE *Gynaecology*

Putative human myometrial and fibroid stem-like cells have mesenchymal stem cell and endometrial stromal cell properties

Amanda L. Patterson[1,2], Jitu W. George[1], Anindita Chatterjee[1], Tyler J. Carpenter[1], Emily Wolfrum[3], and David W. Chesla[1,4], and Jose M. Teixeira[1,*]

[1]Department of Obstetrics, Gynecology and Reproductive Biology, College of Human Medicine, Michigan State University, Grand Rapids, MI 49503, USA [2]Division of Animal Sciences and Department of Obstetrics, Gynecology and Women's Health, University of Missouri, Columbia, MO 65203, USA [3] Bioinformatics and Biostatistics Core, Van Andel Research Institute, Grand Rapids, MI 49503, USA [4]Office of Research, Spectrum Health, Grand Rapids, MI 49503, USA

*Correspondence address. MSU Ob/Gyn, 400 Monroe Ave NW, Room 3006, Grand Rapids, MI 49503, USA. E-mail: jose.teixeira@hc.msu.edu

Submitted on September 25, 2019; resubmitted on October 8, 2019; editorial decision on October 23, 2019

STUDY QUESTION: Can endometrial stromal stem/progenitor cell markers, SUSD2 and CD146/CD140b, enrich for human myometrial and fibroid stem/progenitor cells?

SUMMARY ANSWER: SUSD2 enriches for myometrial and fibroid cells that have mesenchymal stem cell (MSC) characteristics and can also be induced to decidualise.

WHAT IS KNOWN ALREADY: Mesenchymal stem-like cells have been separately characterised in the endometrial stroma and myometrium and may contribute to diseases in their respective tissues.

STUDY DESIGN, SIZE, DURATION: Normal myometrium, fibroids and endometrium were collected from hysterectomies with informed consent. Primary cells or tissues were used from at least three patient samples for each experiment.

PARTICIPANTS/MATERIALS, SETTING, METHODS: Flow cytometry, immunohistochemistry and immunofluorescence were used to characterise tissues. *In vitro* colony formation in normoxic and hypoxic conditions, MSC lineage differentiation (osteogenic and adipogenic) and decidualisation were used to assess stem cell activity. Xenotransplantation into immunocompromised mice was used to determine *in vivo* stem-like activity. Endpoint measures included quantitative PCR, colony formation, trichrome, Oil Red O and alkaline phosphatase activity staining.

MAIN RESULTS AND THE ROLE OF CHANCE: $CD146^+CD140b^+$ and/or $SUSD2^+$ myometrial and fibroid cells were located in the perivascular region and formed more colonies *in vitro* compared to control cells and differentiated down adipogenic and osteogenic mesenchymal lineages *in vitro*. $SUSD2^+$ myometrial cells had greater *in vitro* decidualisation potential, and $SUSD2^+$ fibroid cells formed larger tumours *in vivo* compared to control cells.

LARGE-SCALE DATA: N/A

LIMITATIONS, REASONS FOR CAUTION: Markers used in this study enrich for cells with stem/progenitor cell activity; however, they do not distinguish stem from progenitor cells. $SUSD2^+$ myometrial cells express markers of decidualisation when treated *in vitro*, but *in vivo* assays are needed to fully demonstration their ability to decidualise.

WIDER IMPLICATIONS OF THE FINDINGS: These results suggest a possible common MSC for the endometrial stroma and myometrium, which could be the tumour-initiating cell for uterine fibroids.

STUDY FUNDING/COMPETING INTEREST(S): These studies were supported by NIH grants to JMT (R01OD012206) and to ALP (F32HD081856). The authors certify that we have no conflicts of interest to disclose.

Key words: mesenchymal stem cells / myometrium / fibroids / stem/progenitor cells / endometrial stromal stem/progenitor cells

Introduction

Uterine fibroids (leiomyomas) are benign smooth muscle tumours of the myometrium and are the most common gynaecological tumour, occurring in up to 75% of women in the USA, depending on race or ethnicity (Laughlin and Stewart, 2011; Walker and Stewart, 2005). Approximately 25% of these women present with clinically significant fibroids (Laughlin and Stewart, 2011). Although some medical treatments exist and have been shown to alleviate some symptoms, most are not suitable for long-term treatment, have variable side effects and do not reduce fibroid burden. For example, in one study levonorgestrel (Mirena®) reduced excessive bleeding and obviated the need for hysterectomy in the majority of patients (Machado *et al*., 2013); however, another study had contradictory results (Mercorio *et al*., 2003). Because of fibroid-associated morbidities and the lack of efficacious, long-term therapeutic options, hysterectomy is often the only option for many women, unfortunately resulting in sterility. Fibroids are the most common indication for hysterectomy in the USA and account for approximately half of the 600 000 hysterectomies performed annually (Farquhar and Steiner, 2002; Wu *et al*., 2007). Despite the high prevalence of uterine fibroids, the associated morbidities and the significant healthcare burden they pose, very little is known about the etiology and pathogenesis of the disease, which is a major impediment to development of novel therapies to prevent or treat the disease.

Adult somatic stem cells are responsible for tissue homeostasis in many tissues through their ability to self-renew and produce lineage-differentiating daughter cells by asymmetric division (Blanpain and Fuchs, 2009; Biteau *et al*., 2011). Likewise, tumour-initiating cells, often thought of as tumour/cancer stem cells, are proposed to initiate and maintain tumours also by self-renewal and differentiation (Qureshi-Baig *et al*., 2017; Zhou *et al*., 2009). Because of the remarkable plasticity of the uterus during the menstrual cycle, pregnancy and postpartum uterine involution, it is reasonable to propose the existence of somatic stem cells within the tissue (Teixeira *et al*., 2008) and that mutation or dysregulation of one of these cells could give rise to tumours including uterine fibroids, especially because fibroids are likely clonal (Canevari *et al*., 2005; Zhang *et al*., 2006; Holdsworth-Carson *et al*., 2014).

The perivascular and mesenchymal stem cell (MSC) markers CD146 and CD140b as well as SUSD2 have been used in combination or individually to enrich for putative endometrial stromal MSCs (Schwab and Gargett, 2007; Masuda *et al*., 2012). For the myometrium, investigators have used various combinations of surface markers, including CD34/CD49f/b (Ono *et al*., 2015), CD44/Stro-1 (Mas *et al*., 2015) or other techniques, including Hoechst dye exclusion (side population analysis) (Ono *et al*., 2007; Chang *et al*., 2010), to enrich for putative myometrial MSCs. These studies would suggest a separate MSC population for each of the endometrial stromal and the myometrial tissues. However, because the endometrial stroma and the myometrium originate from the same embryonic tissue, the Müllerian duct mesenchyme (Teixeira *et al*., 2008), we hypothesise that they contain MSCs with a common lineage and that these cells could contribute to a wide variety of mesenchymal cell diseases including uterine fibroids. We have begun testing this hypothesis by using CD146/CD140b and SUSD2 to characterise, isolate and functionally test the stem cell qualities of these cells from myometria and uterine fibroids.

Materials and Methods

Human tissue collection

Use of human tissue specimens was approved by the Michigan State University Institutional Review Board. Matched samples of 'normal' myometrium, fibroids (<8 cm) and endometrium (Endo) were obtained from pre-menopausal, self-identified Caucasian and African American women, undergoing hysterectomy for treatment of uterine fibroids. The patients gave consent to donate through the Spectrum Health Biorepository. Specimens from women with prior use of progestins were compared with non-treated (NT) women and determined to not be different in terms of the percentage of $SUSD2^+$ or $CD146^+CD140b^+$ cells present in the tissue (Fig. S1C and D). Therefore, these samples were not excluded from experiments but were monitored for any outlier differences in subsequent assays, for which none were found.

Cell isolation, magnetic bead separation and flow cytometry

For isolation of SUSD2-expressing cells, tissue samples were minced, placed in digestion media (DMEM/F12, Thermo Fisher, Waltham, MA) containing antibiotic–antimycotic, foetal bovine serum, collagenase type I, DNase type I (Sigma) and $MgCl_2$ and incubated at 37°C overnight with agitation. Endo cells were similarly isolated but with a 1–2-h digestion time. The resulting cell suspensions were strained through 100- and 40-µm meshes, washed with PBS and centrifuged. The cell pellets were resuspended in ACK Lysis Buffer (Thermo Fisher), washed and centrifuged again. Cells were either plated for expansion or processed immediately for magnetic bead separation. Following depletion of dead cells using the Dead Cell Removal Kit (Miltenyi Biotec, Auburn, CA) per manufacturer's instructions, cells were separated by SUSD2 expression using the MACS MicroBeads system (Miltenyi Biotec). Briefly, cells were incubated with anti-SUSD2-PE antibody (Miltenyi Biotec #130-106-325), diluted in staining buffer (PBS, BSA, EDTA), washed and then incubated with anti-PE MicroBeads in staining buffer. After washing and resuspending, cells were passed over MS or LS Columns (Miltenyi Biotec), separated into tubes as $SUSD2^-$ or $SUSD2^+$ cells and used for downstream applications. Purity of separated cell populations was verified by flow cytometry. Events were gated initially by forward and side scatter, then for singlets (side scatter area × height) and finally for phycoerythrin (PE) fluorescence using FlowJo software (FlowJo, Ashland, OR). Unseparated, unstained cells served as a gating control (Fig. S1A).

For isolation of CD146- and CD140b-expressing cells, myometrial and fibroid tissues were minced and digested for 1–2 h using the MACS Human Tumor Dissociation Kit and gentleMACS Dissociator (Miltenyi Biotec) as per the manufacturer's instructions for tough tumours. Following dissociation, cells were processed as above for cell sorting by suspension in staining buffer with FBS and anti-CD146-PE (BD Biosciences, San Jose, CA, #550315) and anti-CD140b-APC (BioLegend, #323608) antibodies, washed and incubated with 300 nM DAPI. Cells were resuspended in staining buffer and analysed on a MoFlo Astrios Flow Cytometer (Beckman Coulter, Brea, CA). Events were gated by forward and side scatter, for singlets (forward scatter height × area), for live cells ($DAPI^-$) and finally for CD146-PE and CD140b-APC expression using Summit Software System (Cytomation,

Fort Collins, CO). The following cell populations were sorted: (i) $CD146^+CD140b^+$ cells and (ii) depleted (remaining cells depleted of $CD146^+CD140b^+$ cells). Unstained cells and fluorescence minus one (FMO) were used as gating controls. Flow cytometry analyses are presented using FlowJo (Fig. S1B).

In vitro assays

Colony formation

After isolation and selection for either SUSD2 expression ($SUSD2^+$ or $SUSD2^-$) or CD146 and CD140b expression ($CD146^+CD140b^+$ or depleted), cells were plated at colony forming density (50 cells/cm^2) in duplicate and grown in MesenPro RS (Thermo Fisher) for 3 weeks. Cultures were fixed in 4% paraformaldehyde (PFA) and stained with crystal violet to visualise colonies. Colonies with $\geq$50 cells were counted, and the percent colony-forming units (CFUs) was calculated as (number of colonies/number of cells plated) $\times$ 100 and averaged for duplicates. For oxygen tension experiments, cells were separated based on SUSD2 expression and cultured as described above, or under 20% O_2 (normoxic) or 2% O_2 (hypoxic) conditions. Cultures were grown until colonies with $\geq$50 cells were visible at which time they were stopped and stained with crystal violet. Matched $SUSD2^-$ and $SUSD2^+$ populations were cultured in different wells of the same plate, and therefore culture was stopped for both cell types on the same day. The number of days to colony formation and the %CFUs were calculated as well as the rate of colony formation as %CFU/days. Images were taken using a Nikon SMZ18 microscope and Ds-Ri1 camera (Nikon Instruments Inc.).

Mesenchymal lineage differentiation

For osteogenic and adipogenic differentiation, cells were plated at 50% confluency in growth media (DMEM/F12, 10% FBS, 1$\times$ antibiotics/antimycotics) and grown to 90% confluency, without passage ($\sim$3–5 days), to obtain enough live cells for differentiation experiments. Following enrichment for $SUSD2^+$, cells were plated in 24-well plates in duplicate and cultured in StemPro Adipogenesis Differentiation or StemPro Osteogenesis Differentiation (Thermo Fisher Scientific) media according to the manufacturer's instructions. Cells were cultured in regular growth media to serve as differentiation controls. To assay adipogenic differentiation, cultures were fixed in 4% PFA, stained using Oil Red O, prepared as described in Lonza's protocol (WEB-PR-PT-2501OIL-3), for 1 h, and counterstained with hematoxylin. To assay osteogenic differentiation, cultures were stained for alkaline phosphatase activity using the Alkaline Phosphatase (AP), Leukocyte kit (Sigma) according to the manufacturer's instructions, adapted for 24-well culture plates. For smooth muscle differentiation, 15×10^3 cells were plated on 1 mg/ml dried rat tail collagen (Corning 354 236) and grown in Medium 231 with a smooth muscle differentiation supplement (Thermo Fisher). Media was changed the following day after plating. Cultures were fixed in 4% PFA at the indicated times and stained using αSMA-Cy3 (Sigma). Images were taken using a Nikon Eclipse Ni-U or Nikon SMZ18 microscope and Ds-Qi1MC or Ds-Ri1 camera (Nikon Instruments Inc.).

Decidualisation

Myometrial cells were expanded in culture, separated based on SUSD2 expression as described above, then seeded at 10^6 cells/well in a 6-well plate and cultured overnight in phenol red-free DMEM/F12 with 10% charcoal dextran-stripped FBS (CDS-FBS) and antibiotics/antimycotics. To induce decidualisation, the following day, cells were switched to 2% serum with or without a decidualisation cocktail consisting of 36 nM 17β-estradiol (Sigma), 1 µM medroxyprogesterone 17-acetate (Sigma) and 0.5 mM dibutyryl-cAMP (Sigma) (Olson *et al.*, 2017). Primary human Endo cells were isolated as described above and cultured and passaged to deplete epithelial cells but not separated by SUSD2 expression, to serve as a positive control for decidualisation induction. All cultures were continued for 5–8 days, with media replenished every third day, and then processed for expression of *IGFBP1*, *MME* and *PRL* mRNA (see below).

Xenotransplantation

Guidelines for animal welfare were followed, and the Michigan State University Institutional Animal Care and Use Committee approved the experiments involving animals. Fibroid cells were isolated, expanded in culture and separated by SUSD2 expression as described above. $SUSD2^-$ and $SUSD2^+$ cell pellets were formed as described (Kurita and Serna, 2018). Briefly, 0.25–0.5 $\times$ 10^6 cells were suspended in 20 µL Rat Tail Collagen I (Corning, Corning, NY, USA) solution and allowed to solidify. Growth media were added to each well, and pellets were cultured for 1–5 days until contraction resulted in a diameter of $\leq$0.5 mm in diameter. $SUSD2^-$ and $SUSD2^+$ cell pellets were grafted under opposing renal capsules of adult female ovariectomized NSG (NOD-SCID (*IL2R*γ^{null})) mice implanted with a 17β-estradiol (0.05 mg) + progesterone (50 mg) 60-day release hormone pellet (Innovative Research of America, Sarasota, FL). After 1–2 months, mice were euthanized and kidneys with grafts were collected, fixed in 4% PFA and embedded in paraffin. Prior to fixation, grafts were imaged using a Nikon SMZ18 microscope and Ds-Ri1 camera (Nikon Instruments Inc.).

Gelatin embedding and frozen tissue preparation

Unfixed tissues were incubated overnight at 4°C in 15% sucrose buffered in PBS. The following day tissues were incubated for at 37°C in a gelatin mix (15% sucrose, 7.5% gelatin in PBS), embedded on a cold block, frozen in isopentane. Tissues were cryo-sectioned at 6–8 µm and thaw mounted. Slides were prepared for immunofluorescence staining by gelatin removal in 37°C PBS.

Immunofluorescence and immunocytochemistry

Sections were incubated in blocking solution (0.1% Triton X-100, 0.1% BSA and 10% serum in PBS), followed by primary antibody diluted in blocking solution overnight at 4°C. The following day, tissues were incubated with a secondary antibody diluted in blocking solution, then counterstained with 4′,6-diamidino-2-phenylindole (DAPI; BioLegend, San Diego, CA, USA), and coverslipped with Fluoro-Gel (Electron Microscopy Sciences (EMS), Hatfield, PA). Omission of primary antibodies served as a negative control. Immunocytochemistry for IGFB1, CD10 and aSMA was performed essentially as described in (Mukherjee *et al.*, 2018). The following primary antibodies were used: aSMA (1:1000; Sigma #), CD140b (1:100; Abcam, Cambridge, MA, #ab69506), CD146 (1:100, Millipore, Burlington, MA, #04-1147),

CD31 (1:100; Thermo Fisher #RB-10333), CD31 (1:100; Abcam #ab9498), SUSD2 (1:100; BioLegend #327401) and IGFBP1 (1:1000; Thermo Fisher #PAS61388). Secondary antibodies used were goat anti-rabbit Alexa Fluor 568 or 647 and goat anti-mouse Alexa Fluor 546 (Thermo Fisher) all at 1:1000. Images were taken using a Nikon Eclipse Ni-U microscope and Ds-Qi1MC monochrome camera (Nikon Instruments Inc., Melville, NY) and pseudocolourised.

Cell viability

The percentage of live cells was determined by hemocytometer counting of Trypan Blue-negative cells. Cells were counted following flow cytometry sorting of DAPI negative (i.e. live), depleted (control) and CD146$^+$CD140b$^+$ (enriched) cells and after dead cell removal and after magnetic bead separation of SUSD2$^-$ (control) and SUSD2$^+$ (enriched) cells.

RNA extraction, cDNA synthesis and qRT-PCR

Total RNA was extracted from cells that underwent *in vitro* decidualisation and controls using the RNeasy Plus Micro Kit (Qiagen, Germantown, MD, USA) per manufacturer's instructions. RNA was reverse-transcribed using SuperScript IV Reverse Transcriptase (Thermo Fisher Scientific) with oligo-dT primers. Quantitative real time-PCR (qRT-PCR) was then performed for *IGFBP1*, *PRL,* CD10 *(MME)* and *RPL17* with primer sets (0.2 µM final concentration each) listed in Supplementary Table S1, using Power SYBR Green Master Mix (Applied Biosystems, Foster City, CA, USA) by a ViiA 7 Real-Time PCR System (Applied Biosystems). For αSMA (*ACTA2*) expression, SUSD2$^+$ myometrial cells were taken prior to plating for RNA isolation and after differentiation for expression of αSMA mRNA as above with the primer set listed in Supplementary Table S1. The $2^{-\Delta\Delta CT}$ method was used to calculate fold change of treated compared to untreated cells after normalising to *RPL17*.

Trichrome staining

Paraffin-embedded kidney-tumour grafts were sectioned at 6 µm and rehydrated through a graded ethanol series. Tissues were then processed for trichrome staining following the manufacturer's instructions (Sigma, cat. #HT15-1KT) to detect collagen (blue stain) compared to cytoplasm and muscle fibres (red). After dehydration, mounting and coverslipping, images were taken using a Nikon Eclipse Ni-U microscope and Ds-Qi1MC camera (Nikon Instruments, Inc.).

Statistical analyses

Statistical analyses were performed using GraphPad Prism 7 (GraphPad, La Jolla, CA, USA) with significance assigned at $P \leq 0.05$ unless otherwise indicated in figure legends. Normality was performed by the Shapiro–Wilk test. For Fig. 2, Wilcoxon matched-pairs signed-rank test was used for (C), unpaired *t* test with equal SD was used for (F), and paired *t* test with equal SD was used for (I), In Fig. 3, paired *t* test with equal SD was used for (C) and (F). For panel (G), a Poisson-mixed-effects model with a random intercept for each individual was used to determine if flow versus bead data differed significantly. Kendall's tau was also used to determine the level of concordance between both of these methods. A result of 0 = no evidence of concordance; 1 = evidence of complete concordance; −1 = evidence of complete discordance. Data in Fig. 4E and J and Supplementary Figure S2A and C were analysed in R (v 3.6.0). Percent values were transformed using a previously described method (Team 2018). Beta mixed-effects models with an interaction term for normoxic/hypoxic condition and SUSD2$^{+/-}$ status and a random effect for patient were used to assess the transformed data (Smithson and Verkuilen, 2006). The package emmeans was used to test specific contrasts of interest (https://CRAN.R-project.org/package=emmeans). Note: the results are given on the logit scale, not the response scale. Ratio paired *t* test with equal SD was used for all analyses in Figs 6 and 7. For Supplementary Figure S1, Mann–Whitney test was used for (C) and unpaired *t* test with equal SD was used for (D). Paired *t* test with equal SD was used for Supplementary Figure S2. Sample sizes are indicated in the figure legends.

Results

Characterisation of CD146$^+$CD140b$^+$ and SUSD2$^+$ cells in myometrium and fibroids

CD146, CD140b and SUSD2 can mark perivascular cells and also enrich for putative MSCs, which localise to the perivascular region in various tissues (Crisan *et al*., 2008; Feng *et al*., 2010; Sivasubramaniyan *et al*., 2013; Lv *et al*., 2014; Wong *et al*., 2015; Lee *et al*., 2016). Specifically in human endometrial stroma, CD146$^+$CD140b$^+$ cells (Schwab and Gargett, 2007) and SUSD2$^+$ cells (Masuda *et al*., 2012) are predominantly perivascular, so we therefore wanted to determine the location of these cells in myometrial and fibroid tissues. Similarly to the endometrial stroma (Darzi *et al*., 2016; Masuda *et al*., 2012), SUSD2 was almost exclusively expressed by perivascular cells in myometria (Fig. 1A–C) and fibroids (Fig. 1D–F). CD146 and CD140b co-expressing cells (CD146$^+$CD140b$^+$) were also predominantly located in the perivascular region in myometria (Fig. 1G–L) and fibroids (Fig. 1M–R), which is consistent with their location in endometrial stroma (Darzi *et al*., 2016; Schwab and Gargett, 2007).

Flow cytometry was used to quantify the percentages of SUSD2$^+$ and CD146$^+$CD140b$^+$ cells present within matched tissue samples, which averaged 38% SUSD2$^+$ (Fig. 2A and C) and 25% CD146$^+$CD140b$^+$ (Fig 2D and F) cells in myometria. These populations did not vary significantly by stage of the menstrual cycle or in the case of progestin treatment (Fig. S1C). In fibroids, approximately 13% of the cells were SUSD2$^+$ (Fig. 2B and C) and 16% were CD146$^+$CD140b$^+$ (Fig. 2E and F), which also did not vary significantly by stage of the menstrual cycle or by progestin treatment (Fig. S1D). By both SUSD2 expression and CD146/CD140b co-expression, a significantly lower percentage of cells were present in fibroids compared to matched myometria (Fig. 2C and F). Concomitantly, a decrease in CD31 expression, which marks vascular endothelial cells, was also seen in fibroids by flow cytometry suggesting fewer vessels in that tissue (Fig. 2G–I).

CD146$^+$CD140b$^+$ and SUSD2$^+$ myometrial cells are enriched for colony-forming units

A hallmark of MSCs is the ability to form colonies *in vitro*, which displays their self-renewal capacity (Bianco *et al*., 2008; Vemuri *et al*., 2011). We used this assay to determine whether the SUSD2$^+$ and CD146$^+$CD140b$^+$ myometrial cell fractions were enriched

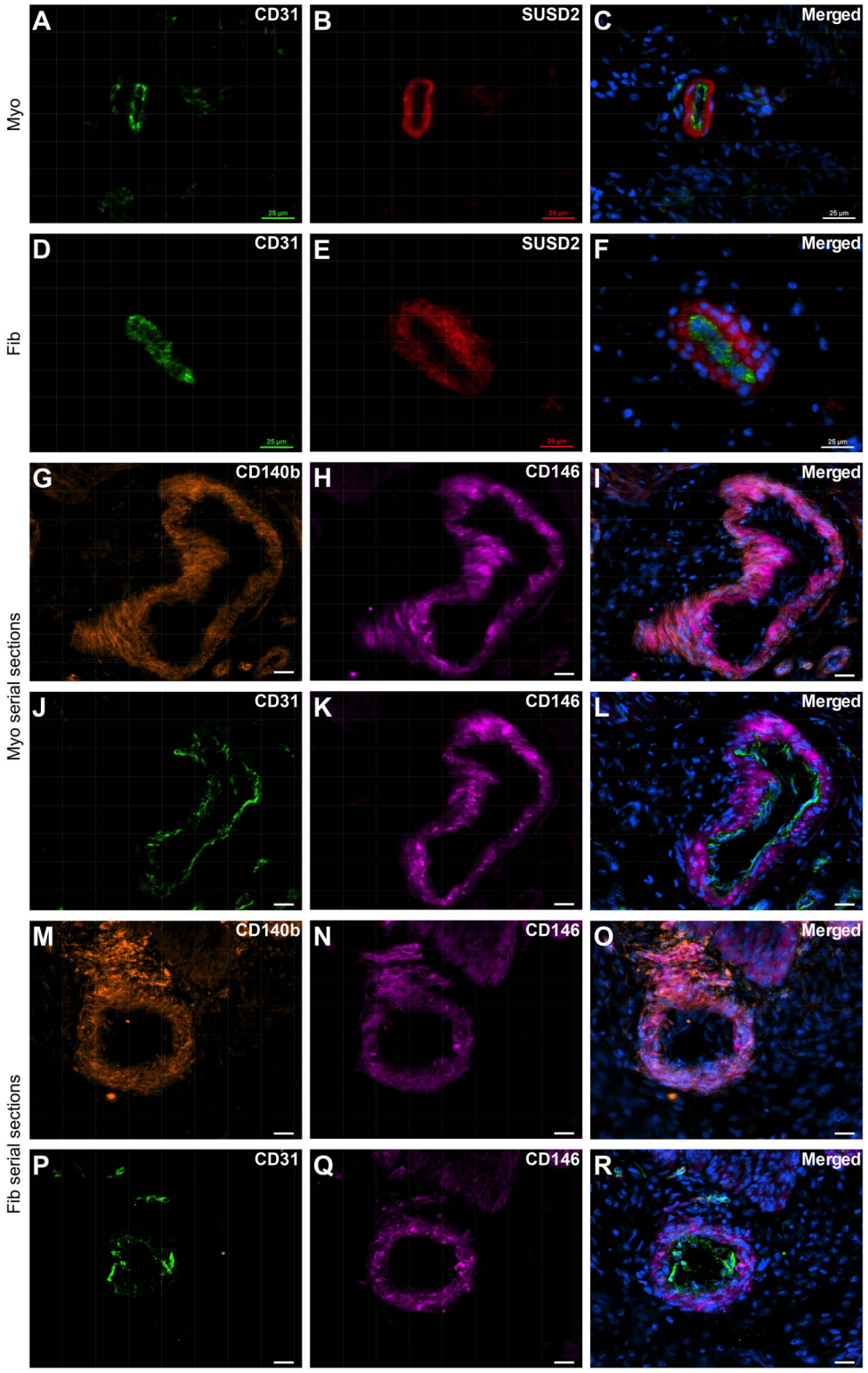

Figure 1 Localisation of SUSD2$^+$ and CD146$^+$CD140b$^+$ cells in myometrium and fibroid tissues. Immunofluorescence analyses were performed on frozen tissue sections to localise putative MSC markers. SUSD2 expression (**B**, **E**) is primarily localised to the perivascular region surrounding CD31$^+$ endothelial cells (**A**, **D**) in myometrial (A–**C**) and fibroid (D–**F**) tissue. (**G**–**I**) CD146 and CD140b co-expressing cells in myometrium tissue. (**J–L**) serial section to (G–I) showing CD31$^+$ endothelial cells with surrounding CD146$^+$ perivascular cells. (**M–O**) CD146 and CD140b co-expressing cells in fibroid tissue and (**P–R**) serial section showing CD31$^+$ endothelial cells with surrounding CD146$^+$ perivascular cells. Scale bars are 25 μM; nuclei are shown stained with DAPI in merged images, which are representative of $n = 5$ patient samples.

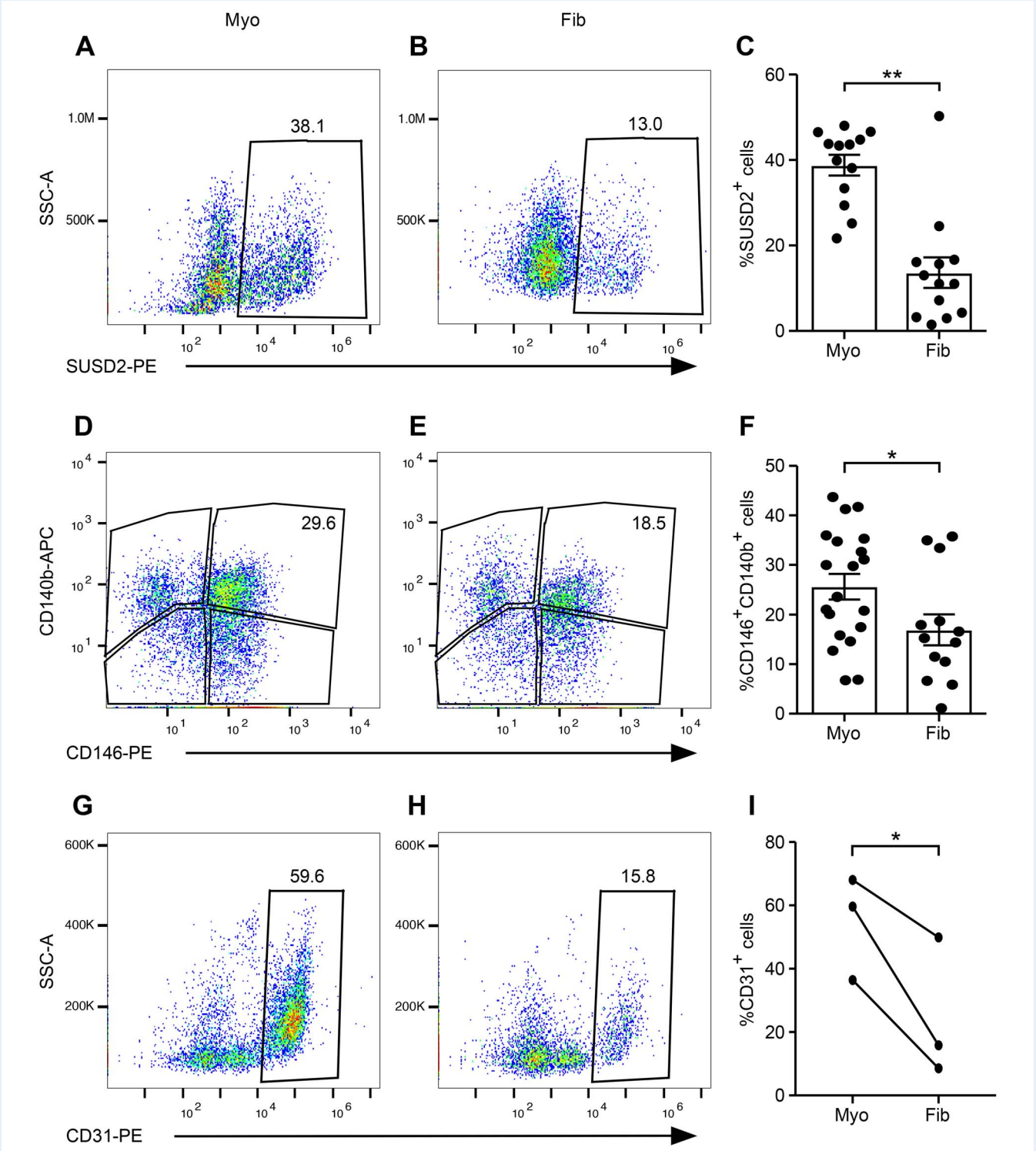

Figure 2 Flow cytometry characterisation of myometria and fibroids. Representative flow cytometry scatter plots of SUSD2 (**A**, **B**), CD146/CD140b^{-} (**D**, **E**) and CD31^{-} (**G**, **H**) expressing cells are shown in myometrial (A, D, G) and fibroid (B, E, H) tissues. Graphs show the percentages of SUSD2^{+} [(**C**), n = 13, Wilcoxon matched-pairs signed-rank test, P = 0.004], CD146^{+}CD140b^{+} [(**F**), n = 20 myometria, n = 13 fibroids, unpaired t test with equal SD, P = 0.04], and CD31^{+} [(**I**) (n = 3, paired t test with equal SD, P = 0.05] cells in myometrial and fibroid samples. Error bars are ± SEM. SSC-A, side scatter area, PE, phycoerythrin, APC, allophycocyanin.

for colony-forming units (CFUs). Both SUSD2$^+$ (Fig. 3A–C) and CD146$^+$CD140b$^+$ (Fig. 3D–F) populations had significantly higher percentages of CFUs compared to the corresponding controls. Our preliminary observations suggested that myometrial cell viability was compromised following flow cytometry cell sorting. We therefore determined the percentage of live cells after bead separation and flow cytometry sorting. As suspected, significantly fewer live cells were present in the depleted and CD146$^+$CD140b$^+$ flow cytometry sorted cells compared to the SUSD2$^-$ and SUSD2$^+$ magnetic bead separated cells (Fig. 3G).

Our initial observations of SUSD2$^+$ and CD146$^+$CD140b$^+$ cells revealed similar expression profiles by immunofluorescence (Fig. 1) and flow cytometry (Fig. 2) and comparable colony-forming efficiencies (Fig. 3). However, because viability of flow cytometry-sorted CD146$^+$CD140b$^+$ cells was decreased compared to bead-separated SUSD2$^+$ cells (Fig. 3G) and due to ease of isolation, we chose to use magnetic bead separation by SUSD2 for all subsequent experiments.

Colony-forming activity of SUSD2$^+$ myometrial and fibroid cells is affected by oxygen tension

Our initial attempts to assess the percentage of CFUs in SUSD2$^+$ and SUSD2$^-$ fibroid cells resulted in no colonies being formed (data not shown) after 3 weeks of culture, which was the amount of time needed for myometrial cells to form colonies. We therefore decided to compare normal versus low oxygen (O_2) levels because hypoxia has been shown to exert growth-promoting effects on rat (Lennon *et al*., 2001) and human (Grayson *et al*., 2006) MSCs. We also allowed the cultures to continue until colonies formed (rather than stopping the experiment at a pre-determined time) because fibroids have been shown to have variable growth rates compared to the myometrium (Loy *et al*., 2005; Holdsworth-Carson *et al*., 2016) and may require more time to form colonies *in vitro*. To determine if cells grown in low O_2 (2%, Hypox) form colonies faster than in normal O_2 (20%, Normox), we attempted to keep the number of colonies formed constant and let time (days) to formation be the variable. To do this, we allowed cultures to continue until a similar number of colonies formed in matched populations (e.g. similar number of colonies in myometrial SUSD2$^+$ cultures in Normox and Hypox) and then counted the number of days and colonies. The rate of colony formation was calculated as %CFUs/days. For myometrial cells, there was a significant difference in the rate of colonies formed between Normox and Hypox for both SUSD2$^-$ (Fig. 4A, B and E) and SUSD2$^+$ cells (Fig. 4C–E). This was shown to be due to a difference in the number of days required to form colonies (Fig. S2B), not the %CFUs formed in Normox compared to Hypox conditions (Fig. S2A). For fibroid SUSD2$^-$ cells, there was not a significant difference in the rate of colony formation in Normox and Hypox conditions (Fig. 4F, G and J). Remarkably, three out of four SUSD2$^-$ samples did not form any colonies after 5+ weeks in culture regardless of O_2 levels, even though the matched SUSD2$^+$ cells did. SUSD2$^+$ fibroid cells grown in Hypox required fewer days to form colonies (Fig. S2D), and the rate of colony formation was significantly higher in Hypox compared to Normox conditions (Fig. 4J). Because matched SUSD2$^-$ and SUSD2$^+$ cells were cultured on the same plates in either Normox or Hypox conditions, we were able to assess differences in %CFUs from fibroids. This revealed that SUSD2$^+$ cells had significantly higher %CFUs than SUSD2$^-$ cells in Hypox (Fig. S2C). These results suggest that colony formation is more efficient under Hypox compared to Normox conditions.

In vitro differentiation of SUSD2$^+$ myometrial and fibroid cells

Another hallmark of MSCs is their ability to differentiate down various mesenchymal cell lineages including osteoblast, adipocyte, myocyte and chondrocyte (Bianco *et al*., 2008; Vemuri *et al*., 2011). We confirmed that SUSD2$^+$ cells could differentiate into smooth muscle cells on collagen-coated plates in culture with smooth muscle differentiation medium using αSMA expression as an immunofluorescence marker of smooth muscle (Fig. 5A) and by assaying αSMA mRNA induction (Fig. 5B). Collagen was used to provide a stiffness range supportive of myogenic differentiation (Roeder *et al*., 2002; Engler *et al*., 2006; Jayes *et al*., 2019). To examine differentiation to other lineages, SUSD2$^+$ cells were cultured in either control growth media or defined differentiation media and assessed for their ability to differentiate down the adipogenic or osteogenic lineages. SUSD2$^+$ cells from 3/3 myometrial (Fig. 5D) and 2/3 fibroid (Fig. 5F) samples were able to initiate adipogenic differentiation as seen by positive staining for Oil Red O compared to cells grown in control media (Fig. 5C, E). Similarly, staining for alkaline phosphatase activity revealed that all SUSD2$^+$ cell isolates (Fig. 5H and J) were able to undergo osteogenic differentiation compared to cells in control media (Fig. 5G and I).

A characteristic of endometrial stromal cells is their ability to terminally differentiate into decidual cells in a process termed decidualisation that is critical for maintaining early pregnancy (Gellersen and Brosens, 2014). Based on our hypothesis that both the endometrial stroma and myometrium contain stem cells that are derived from the same embryonic Müllerian duct mesenchyme lineage, we examined whether myometrial cells enriched for putative stem/progenitor cells by SUSD2 expression could differentiate into decidual-like cells using a well-defined culture system (Olson *et al*., 2017). SUSD2$^-$ and SUSD2$^+$ myometrial cells and unselected Endo cells (positive control) were treated with a decidualisation-inducing cocktail of estradiol, medroxyprogesterone acetate (MPA) and db-cAMP or were left untreated and then assessed for decidual changes. Decidual cells have been described as epithelial-like in morphology (Gellersen and Brosens, 2014). After 5 days of treatment, a few epithelial-like cells could be seen in the SUSD2$^-$ (Fig. 6B) cultures treated with the decidualisation cocktail compared to the typical spindle-like morphology of the untreated cells (Fig. 6A). However, the changes were much more dramatic in the treated SUSD2$^+$ cultures (Fig. 6C and D) where many large nests of epithelial-like cells could be easily visualised (Fig. 6D), and these also showed granular expression of IGFBP1, a decidualisation marker, and CD10, a stromal cell marker (Fig. 6F, H), which was absent or much less in the control cultures (Fig. 6E, G). At the end of the treatment period, there was increased mRNA expression of the decidual markers, *IGFBP1* and *PRL*, in the SUSD2$^+$ cells compared with SUSD2$^-$ cells (Fig. 6I–J). We also observed increased CD10 (*MME*) mRNA, both in the SUSD2$^+$ cells after decidualisation compared with SUSD2$^-$ cells (Fig. 6K) and over time (Fig. 6L), These results suggest that SUSD2$^+$ myometrial cells can undergo stromal/decidual-like differentiation more efficiently than can SUSD2$^-$ cells.

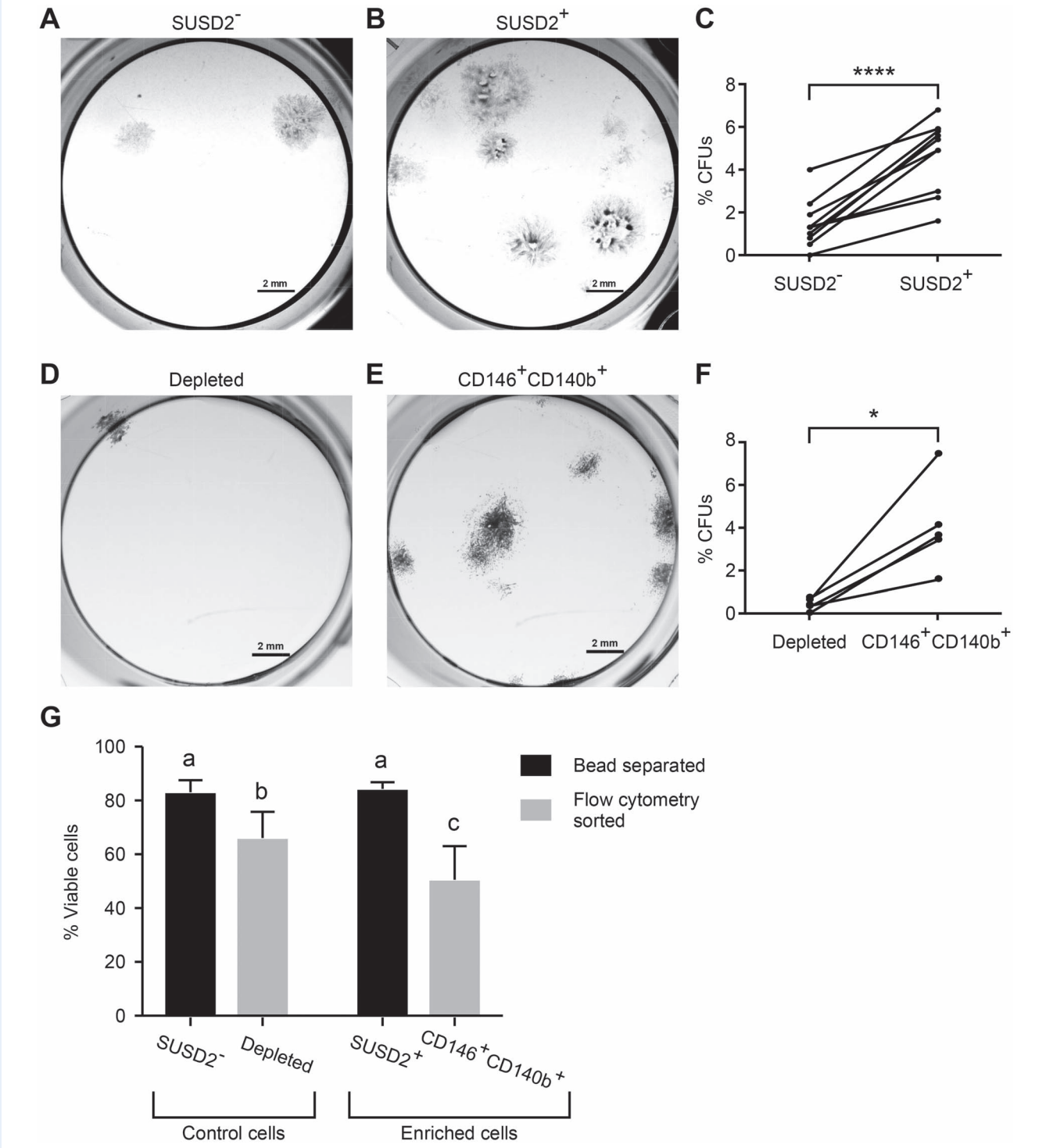

Figure 3 Colony-forming unit (CFU) assay of myometrial cells enriched for SUSD2 or CD146/CD140b expression. Colony formation assays were performed to assess stem cell activity. Representative images are of colonies formed by (**A**) SUSD2$^-$, (**B**) SUSD2$^+$, depleted (**D**) (myometrial cells depleted of CD146$^+$CD140b$^+$ cells) and (**E**) matched CD146$^+$CD140b$^+$ cells. Graphs show the colony forming efficiency represented as %CFUs (colony #/cells seeded × 100) of SUSD2$^-$ and SUSD2$^+$ cells (**C**) ($n = 11$, $P < 0.0001$) and depleted and CD146$^+$CD140b$^+$ cells (**F**) ($n = 5$, $P = 0.016$). Statistical analysis performed by paired t test, error bars are +/− SEM. (**G**) %viable cells by Trypan Blue staining after bead separation of SUSD2$^-$ and SUSD2$^+$ cells ($n = 3$) and after flow cytometry sorting of depleted and CD146$^+$CD140b$^+$ ($n = 4$) were compared using a Poisson-mixed-effects model with a random intercept for each individual to determine whether flow versus bead data differed significantly. Kendall's tau was also used to determine the level of concordance between both of these methods. Different letters indicate significant differences.

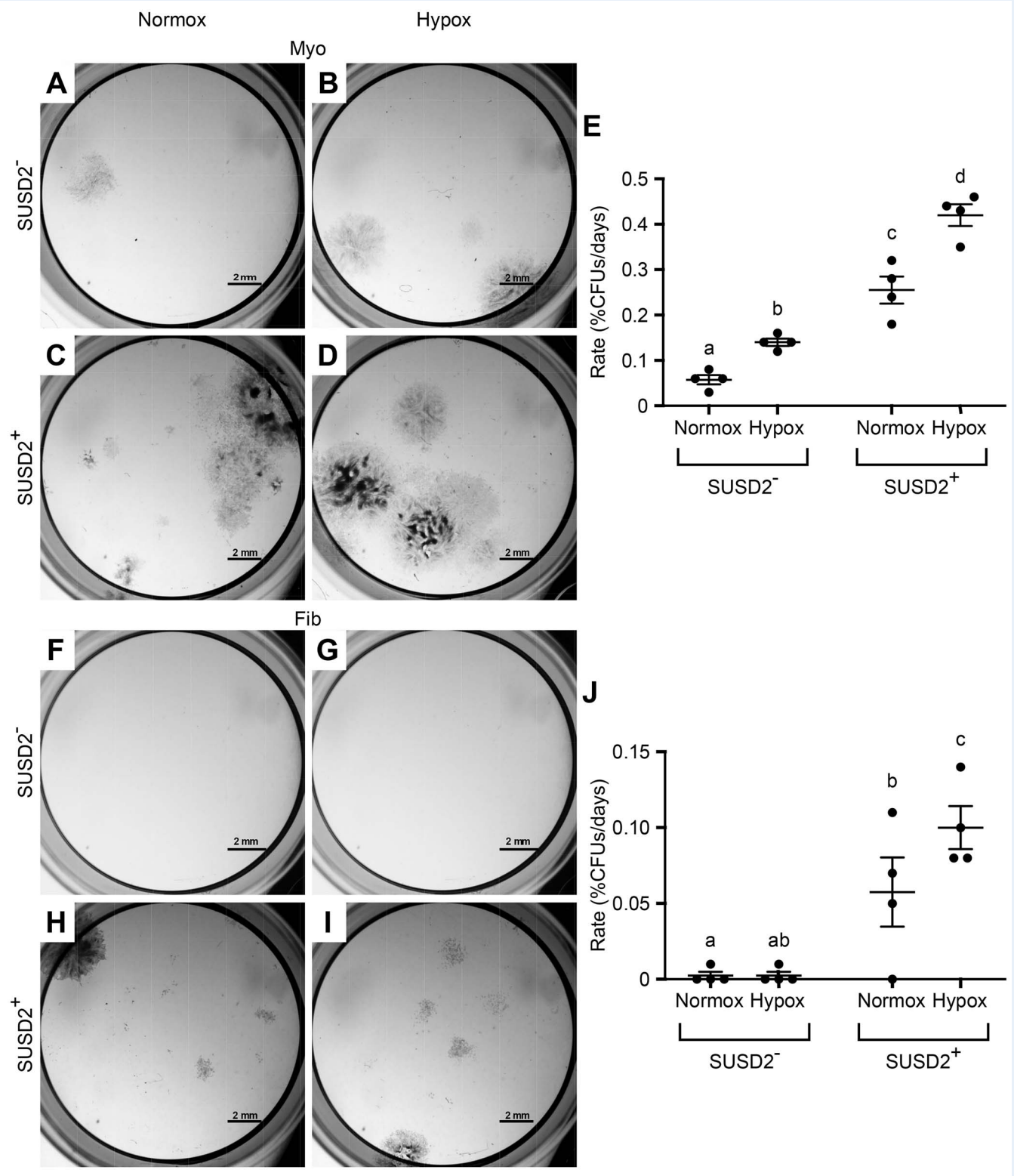

Figure 4 CFU assay of SUSD2$^+$ myometrial and fibroid cells under normoxic and hypoxic conditions. Colony formation assays were performed to assess stem cell activity in normal (20%, Normox) and hypoxic (2%, Hypox) oxygen levels. Representative images are of colonies formed by myometrial (**A**–**D**) and fibroid (**F**–**I**) SUSD2$^-$ (A, B, F, G) and SUSD2$^+$ (C, D, H, I) cells grown under Normox (A, C, F, H) or Hypox (B, D, G, I) conditions. Graphs show the rate of colony forming efficiency represented as %CFUs/days for myometrial (E) and fibroid (**J**) cells. Statistical analysis performed by beta mixed effects with $n = 4$% transformed matched myometrial and fibroid sample values. Different letters indicate significant differences ($P < 0.5$). Error bars are +/− SEM.

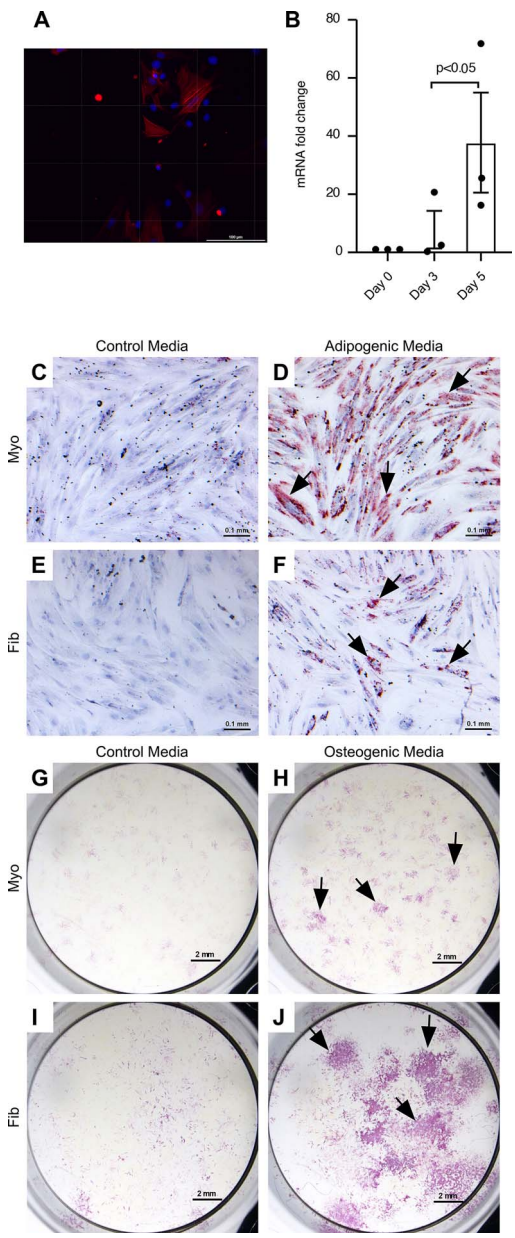

Figure 5 Mesenchymal lineage differentiation of SUSD2+ cells. (**A**) αSMA immunofluorescence in SUSD2+ myometrial cells after differentiation and (**B**) αSMA mRNA fold induction with differentiation. Day 0 represents the SUSD2+ cells before plating. Columns represent the average of $n = 3$ patient myometrial samples. Error bars equal SEM, and ratio paired t test was used to determine significance. Representative images of SUSD2+ myometrial (**C**, **D**, **G**, **H**) and fibroid (**E**, **F**, **I**, **J**) cells grown in control growth media (C, E, G, I) and adipogenic (D, F) or osteogenic (H, J) differentiation media. Adipogenic and control cultures were stained with Oil Red O (red colour, black arrows), and osteogenic and control cultures were stained for alkaline phosphatase activity (purple colour, black arrows). 3/3 myometrial and 2/3 fibroid samples analysed showed adipogenic differentiation. All myometrial and fibroid samples showed osteogenic differentiation. Adipogenic and control cultures were counter stained with hematoxylin. Scale bars are 0.1 mm for αSMA, adipogenic and control cultures and 2 mm for osteogenic and control cultures.

SUSD2+ fibroid cells form tumours *in vivo*

Putative fibroid stem/progenitor cells have been shown to form larger tumours *in vivo* compared to non-stem/progenitor cells (Ono *et al.*, 2012; Yin *et al.*, 2015). We assayed the tumour-forming potential of SUSD2− and SUSD2+ cells from fibroids (Fig. 7A) under opposing renal capsules of immunocompromised (NSG) mice using a well-documented protocol (Kurita and Serna, 2018). Cell pellets were allowed to grow for 1–2 months in mice before analysis. At collection, SUSD2+ cell pellets formed significantly larger tumours compared to SUSD2− cell pellets (Fig. 7B and C). The SUSD2− tumours remained relatively similar in size to the pellets at the time of grafting whereas the SUSD2+ tumours increased in size. Resulting tumours from both SUSD2− and SUSD2+ cells showed distinct collagen deposition by trichrome staining (Fig. 7D–G), and αSMA immunofluorescence (Fig. 7H and J). Interestingly, CD10 immunofluorescence was not detected in any of the xenotransplants (Fig. 7I and J), which might have been expected since the kidney capsule microenvironment is probably not sufficient for supporting decidualisation.

Discussion

We have shown that the markers used to enrich for putative MSCs in the endometrial stroma, CD146/CD140b and SUSD2, similarly enriched for putative MSCs from myometrium and fibroids. These cells were primarily located in the perivascular region, which is where they are located in the endometrial stroma (Schwab and Gargett, 2007; Masuda *et al.*, 2012; Darzi *et al.*, 2016) and is also a stem cell niche for putative MSCs in other tissues (Crisan *et al.*, 2008; Feng *et al.*, 2010; Sivasubramaniyan *et al.*, 2013; Lv *et al.*, 2014; Wong *et al.*, 2015). Of note, the percentage of CD146+CD140b+ and SUSD2+ cells (25 and 38%, respectively) in the myometrium is much higher than what has been reported in the endometrium (CD146+CD140b+ 1.5%, SUSD2+ 4.2%) (Schwab and Gargett, 2007; Masuda *et al.*, 2012). This could be because of the higher density of vasculature in the myometrium compared to the endometrium (Farrer-Brown *et al.*, 1970a; Farrer-Brown *et al.*, 1970b). Similar to other reports of putative myometrial and fibroid MSCs (Ono *et al.*, 2007; Chang *et al.*, 2010, Ono *et al.*, 2014, Ono *et al.*, 2015; Yin *et al.*, 2015), we found significantly fewer CD146+CD140b+ and SUSD2+ cells in fibroids compared to matched myometria.

Others have reported that putative myometrial MSCs proliferated more when cultured in hypoxic conditions compared with those in normal oxygen levels when seeded at a normal density (Ono *et al.*, 2007; Ono *et al.*, 2015) and that putative myometrial and/or fibroid MSCs formed more colonies than non-MSCs specifically under hypoxic conditions (Mas *et al.*, 2012; Mas *et al.*, 2015; Yin *et al.*, 2015). Ours is the first study to assess the colony-forming potential of putative myometrial and fibroid MSCs and non-MSCs seeded at the lowest reported limiting dilution (50 cells/cm^2) in both normal and hypoxic conditions. Interestingly, fibroid SUSD2+ cells took longer and formed fewer colonies than myometrial SUSD2+ cells regardless of oxygen levels, suggesting diminished stem cell activity of the fibroid SUSD2+ population. This leads us to speculate that fibroids grow by stem/progenitor cell differentiation (rather than self-renewal/proliferation) into transient amplifying cells and collagen-depositing cells, resulting in depletion of the stem cell population and consistent with the decreased

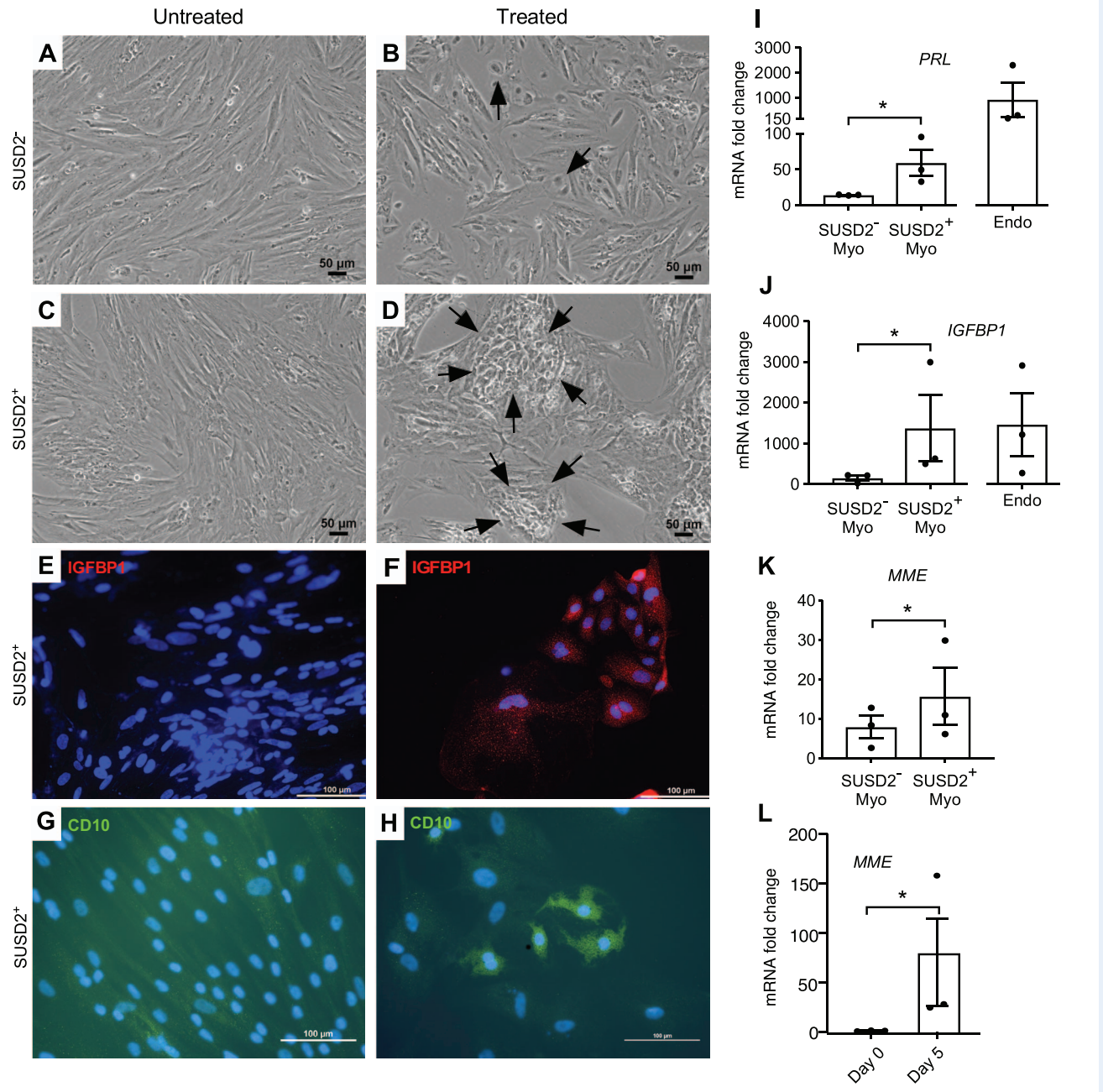

Figure 6 ***In vitro*** **decidualisation of SUSD2$^+$ myometrial cells.** To assess the ability of SUSD2$^+$ and SUSD2$^-$ cells to decidualise, cells were cultured in untreated low serum media or with decidualisation cocktail (E_2, MPA and db-cAMP). Representative images of SUSD2$^-$ (**A**, **B**) and SUSD2$^+$ (**C**, **D**) cells grown in untreated (A, C) or with decidualisation cocktail (B, D) in low serum media after 5 days. Black arrows point to epithelial-like cells in (B) and large epithelial-like nests in (D). Immunocytochemistry for IGFBP1 is shown in (**E**, **F**) and for CD10 in (**G**, **H**). Nuclei are stained with DAPI. Fold induction of mRNA levels for *PRL* (**I**) *IGFBP1* (**J**) and *MME* (CD10) (**K**) of SUSD2$^-$ and SUSD2$^+$ myometrial cells, and endometrial stromal (Endo, control) cells ($n = 3$ each) grown in decidual induction media relative to *RPL17*, and untreated control cells. (**L**) *mRNA* levels of *MME* in SUSD2$^+$ myometrial cells before plating (Day 0) and 5 days after treatment (Day 5) with the decidualisation cocktail. Statistical analysis was performed using the ratio paired *t* test; $^*P < 0.05$. Columns represent mean fold change, and error bars represent SEM. Endo is shown for visual comparison and was not included in the statistical analyses.

percentage of SUSD2$^+$ cells observed in fibroids. Holdsworth-Carson *et al.* (2016) showed that larger fibroids proliferated more than matched myometrium (likely due to highly proliferative transient amplifying cells) and had significantly reduced expression of the stem cell marker, ALDH1A1, suggesting a reduced stem/progenitor cell population. However, when compared to smaller fibroids, large tumours had fewer proliferating cells and substantially more collagen (Flake *et al.*, 2013). Perhaps the Life Cycle hypothesis of fibroid development and growth, which describes phases with both proliferating and non-proliferating myocyte activity, could explain this discrepancy (Flake

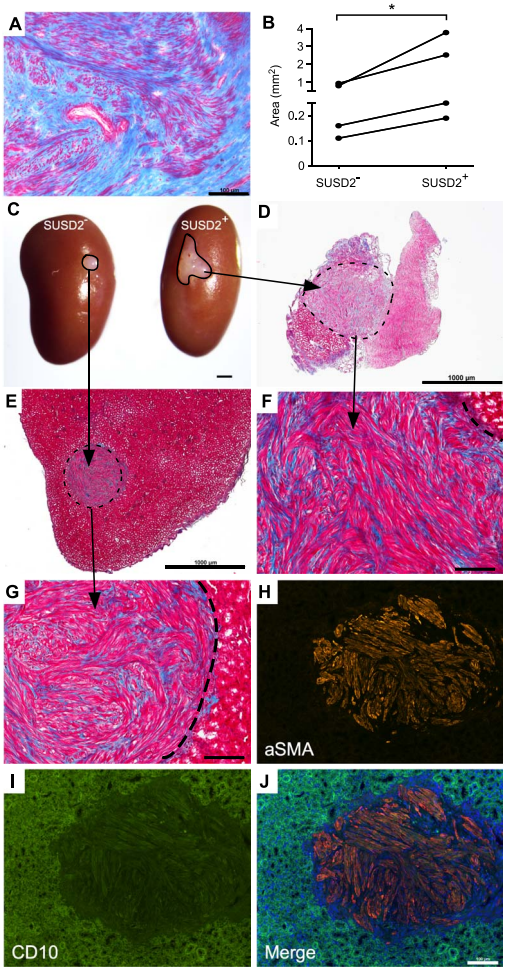

Figure 7 Xenotransplantation and tumour formation of SUSD2+ cells. Xenotransplantation was performed to assess *in vivo* stem cell activity. (**A**) Trichrome staining of the parental fibroid for the xenotransplant images shown in this figure. Red colour shows staining of cytoplasm of muscle cells, and blue shows staining of collagen. Bar = 100 μm. (**B**) Graph of tumour size 8 weeks after transplantation. Statistical analysis performed was ratio paired *t* test for tumour area (mm^2) from SUSD2− and SUSD2+ cells. $*P = 0.038$. (**C**) Representative image ($n = 4$) of fibroid-like tumours that formed from SUSD2− and SUSD2+ cell pellets transplanted under the renal capsule of immunocompromised mice. Representative low magnification images (**D**, **E**; bar = 1 mm) and high-magnification images (**F**, **G**; bar = 100 μm) of trichrome staining of tumours that formed in C. Dotted lines demarcate fibroid-like tumours from kidney tissue. Representative αSMA (**H**) and CD10 (**I**) immunofluorescence images of the fibroid xenotransplants. Green fluorescence observed in the kidney is background fluorescence. Merged αSMA and CD10 image with added DAPI channel shown in (**J**). Bar = 100 μm

et al., 2013). Our results show fewer stem cell activities in fibroid SUSD2+ cells compared to myometria. However, whether the transient amplifying cells in fibroids and/or myometrium are SUSD2+ or SUSD2− has yet to be determined, but we suspect they are SUSD2− because of the greater proliferative capacity of fibroids and the general expectation that stem cells are more quiescent. Indeed, it will be interesting to determine whether the SUSD2+ cells in myometrium and fibroids share characteristics other than those associated with stem cells.

Cells enriched for SUSD2 expression displayed additional *in vitro* stem/progenitor cell activity by multilineage differentiation. SUSD2+ myometrial cells tended to undergo adipogenic differentiation more readily whereas fibroid SUSD2+ cells were more amenable to osteogenic differentiation. This makes some sense, because in a mouse model with loss of β-catenin in the developing myometrium, we have shown that myocytes were converted to adipocytes (Arango *et al.*, 2005) with a possible contribution by label-retaining cells (Szotek *et al.*, 2007). Also, COL1A1 and TGFβ1 which are highly upregulated in uterine fibroids (Malik *et al.*, 2010) are involved in osteogenic differentiation of MSCs (Granchi *et al.*, 2010; Valenti *et al.*, 2016). Therefore, fibroid stem/progenitor cells may be more primed for osteogenic differentiation. We were also able to show *in vivo* stem/progenitor cell activity of fibroid SUSD2+ cells. When grafted under the renal capsules of immunocompromised mice, SUSD2+ cells formed significantly larger tumours compared to SUSD2− cells. This is suggestive of the tumour-initiating properties of SUSD2+ cells similar to what has been hypothesised for other putative cancer/tumour stem/progenitor cells (Zhou *et al.*, 2009; Qureshi-Baig *et al.*, 2017).

In this study, we hypothesised that if SUSD2 expression could enrich for myometrial stem/progenitor cells with a similar identity to endometrial stromal SUSD2+ stem/progenitor cells, they could also be induced to decidualise *in vitro*, which *in vivo* is a phenomenon unique to endometrial stromal cells. We show that myometrial SUSD2+ cells appear to have more potential than the SUSD2− cells to decidualise. To our knowledge, bone marrow-derived MSCs are the only other cell type that can be induced to undergo a decidual-like transformation *in vitro*, whereas a human dermal neonatal fibroblast (HDFn) cell line showed a muted and variable response (Aghajanova *et al.*, 2010). Along with our data, this would suggest that not all fibroblast cells are capable of decidualising *in vitro* but rather it is reserved for more stem-like cells, given they are provided with the appropriate factors.

It warrants noting that although the SUSD2+ population is enriched for cells with stem-like activity, these cells require further characterisation to distinguish stem from progenitor cells. Our data would suggest, based on the high percentage of SUSD2+ cells present in myometrial tissue (~38%) and the higher colony forming efficiency (~4.8%) of these cells compared to other reports of putative stem/progenitor cells (Mas *et al.*, 2012; Mas *et al.*, 2015), that the SUSD2+ population may contain both stem and progenitor cells. Also, fibroids having a smaller percentage of SUSD2+ cells and lower colony-forming potential compared to myometrium may reveal depletion of stem and/or progenitor cells in these tumours.

Historically, it has been proposed that the uterus contains three distinct putative stem cell populations, one for the epithelium, one for the endometrial stroma and one for the myometrium (Teixeira *et al.*, 2008). Our study provides a possible link between putative endometrial stromal and myometrial stem/progenitor cells. Considering that the endometrial stroma and the inner portion of the myometrium in humans both originate from the embryonic Müllerian duct mesenchyme (Noe *et al.*, 1999; Leyendecker, 2000), it is reasonable to propose that a single adult mesenchymal stem/progenitor cell exists for both tissue types. Their respective niches would then regulate differentiation of these cells into either endometrial stromal or myome-

trial smooth muscle cells. These cells may also contribute to uterine diseases, such as uterine sarcomas, endometriosis, adenomyosis and fibroids, in a previously unappreciated way, such that uterine MSCs when mutated or dysregulated could be coaxed to differentiate into either endometrial stromal and myometrial diseases. Determining the existence of a common endometrial stromal and myometrial MSC will shed light onto the potential of this unique cell to contribute to proliferative and tumourigenic diseases.

Supplementary data

Supplementary data are available at *Human Reproduction* online.

Authors' roles

A.L.P.: conception and design, acquisition, analysis and interpretation of data, drafting and revision of manuscript, final approval. J.W.G.: acquisition of data, revision of manuscript, final approval. A.C.: acquisition of data, revision of manuscript, final approval. T.J.C.: acquisition of data, revision of manuscript, final approval. E.W.: analysis, final approval. D.W.C.: acquisition of data, revision of manuscript, final approval. J.M.T.: conception and design, analysis and interpretation of data, revision of manuscript, final approval.

Funding

National Institutes of Health (R01OD012206 to J.M.T., F32HD081856 to A.L.P.).

Conflict of interest

The authors certify that we have no conflicts of interest to disclose.

References

Aghajanova L, Horcajadas JA, Esteban FJ, Giudice LC. The bone marrow-derived human mesenchymal stem cell: potential progenitor of the endometrial stromal fibroblast. *Biol Reprod* 2010;**82**:1076–1087.

Arango NA, Szotek PP, Manganaro TF, Oliva E, Donahoe PK, Teixeira J. Conditional deletion of beta-catenin in the mesenchyme of the developing mouse uterus results in a switch to adipogenesis in the myometrium. *Dev Biol* 2005;**288**:276–283.

Bianco P, Robey PG, Simmons PJ. Mesenchymal stem cells: revisiting history, concepts, and assays. *Cell Stem Cell* 2008;**2**:313–319.

Biteau B, Hochmuth CE, Jasper H. Maintaining tissue homeostasis: dynamic control of somatic stem cell activity. *Cell Stem Cell* 2011;**9**:402–411.

Blanpain C, Fuchs E. Epidermal homeostasis: a balancing act of stem cells in the skin. *Nat Rev Mol Cell Biol* 2009;**10**:207–217.

Canevari RA, Pontes A, Rosa FE, Rainho CA, Rogatto SR. Independent clonal origin of multiple uterine leiomyomas that was determined by X chromosome inactivation and microsatellite analysis. *Am J Obstet Gynecol* 2005;**193**:1395–1403.

Chang HL, Senaratne TN, Zhang L, Szotek PP, Stewart E, Dombkowski D, Preffer F, Donahoe PK, Teixeira J. Uterine leiomyomas exhibit fewer stem/progenitor cell characteristics when compared with corresponding normal myometrium. *Reprod Sci* 2010;**17**:158–167.

Crisan M, Yap S, Casteilla L, Chen CW, Corselli M, Park TS, Andriolo G, Sun B, Zheng B, Zhang L *et al.* A perivascular origin for mesenchymal stem cells in multiple human organs. *Cell Stem Cell* 2008;**3**:301–313.

Darzi S, Werkmeister JA, Deane JA, Gargett CE. Identification and characterization of human endometrial mesenchymal stem/stromal cells and their potential for cellular therapy. *Stem Cells Transl Med* 2016;**5**:1127–1132.

Engler AJ, Sen S, Sweeney HL, Discher DE. Matrix elasticity directs stem cell lineage specification. *Cell* 2006;**126**:677–689.

Farquhar CM, Steiner CA. Hysterectomy rates in the United States 1990-1997. *Obstet Gynecol* 2002;**99**:229–234.

Farrer-Brown G, Beilby JO, Tarbit MH. The blood supply of the uterus. 1. Arterial vasculature. *J Obstet Gynaecol Br Commonw* 1970a;**77**:673–681.

Farrer-Brown G, Beilby JO, Tarbit MH. The blood supply of the uterus. 2. Venous pattern. *J Obstet Gynaecol Br Commonw* 1970b;**77**:682–689.

Feng J, Mantesso A, Sharpe PT. Perivascular cells as mesenchymal stem cells. *Expert Opin Biol Ther* 2010;**10**:1441–1451.

Flake GP, Moore AB, Flagler N, Wicker B, Clayton N, Kissling GE, Robboy SJ, Dixon D. The natural history of uterine leiomyomas: morphometric concordance with concepts of interstitial ischemia and inanosis. *Obstet Gynecol Int* 2013;**2013**: 285103.

Gellersen B, Brosens JJ. Cyclic decidualization of the human endometrium in reproductive health and failure. *Endocr Rev* 2014;**35**:851–905.

Granchi D, Ochoa G, Leonardi E, Devescovi V, Baglio SR, Osaba L, Baldini N, Ciapetti G. Gene expression patterns related to osteogenic differentiation of bone marrow-derived mesenchymal stem cells during ex vivo expansion. *Tissue Eng Part C Methods* 2010;**16**:511–524.

Grayson WL, Zhao F, Izadpanah R, Bunnell B, Ma T. Effects of hypoxia on human mesenchymal stem cell expansion and plasticity in 3D constructs. *J Cell Physiol* 2006;**207**:331–339.

Holdsworth-Carson SJ, Zaitseva M, Vollenhoven BJ, Rogers PA. Clonality of smooth muscle and fibroblast cell populations isolated from human fibroid and myometrial tissues. *Mol Hum Reprod* 2014;**20**:250–259.

Holdsworth-Carson SJ, Zhao D, Cann L, Bittinger S, Nowell CJ, Rogers PA. Differences in the cellular composition of small versus large uterine fibroids. *Reproduction* 2016;**152**:467–480.

Jayes FL, Liu B, Feng L, Aviles-Espinoza N, Leikin S, Leppert PC. Evidence of biomechanical and collagen heterogeneity in uterine fibroids. *PLoS One* 2019;**14**:e0215646.

Kurita T, Serna VA. Patient-derived xenograft model for uterine leiomyoma by sub-renal capsule grafting. *J Biol Methods* 2018;**5**:e91.

Laughlin SK, Stewart EA. Uterine leiomyomas: individualizing the approach to a heterogeneous condition. *Obstet Gynecol* 2011;**117**:396–403.

Lee BJ, Kang DW, Park HY, Song JS, Kim JM, Jang JY, Lee JC, Wang SG, Jung JS, Shin SC. Isolation and localization of mesenchymal stem

cells in human palatine tonsil by W5C5 (SUSD2). *Cell Physiol Biochem* 2016;**38**:83–93.

Lennon DP, Edmison JM, Caplan AI. Cultivation of rat marrow-derived mesenchymal stem cells in reduced oxygen tension: effects on in vitro and in vivo osteochondrogenesis. *J Cell Physiol* 2001;**187**: 345–355.

Leyendecker G. Redefining endometriosis: endometriosis is an entity with extreme pleiomorphism. *Hum Reprod* 2000;**15**:4–7.

Loy CJ, Evelyn S, Lim FK, Liu MH, Yong EL. Growth dynamics of human leiomyoma cells and inhibitory effects of the peroxisome proliferator-activated receptor-gamma ligand, pioglitazone. *Mol Hum Reprod* 2005;**11**:561–566.

Lv FJ, Tuan RS, Cheung KM, Leung VY. Concise review: the surface markers and identity of human mesenchymal stem cells. *Stem Cells* 2014;**32**:1408–1419.

Machado RB, de IM, Beltrame A, Bernardes CR, Morimoto MS, Santana N. The levonorgestrel-releasing intrauterine system: its effect on the number of hysterectomies performed in perimenopausal women with uterine fibroids. *Gynecol Endocrinol* 2013;**29**:492–495.

Malik M, Norian J, McCarthy-Keith D, Britten J, Catherino WH. Why leiomyomas are called fibroids: the central role of extracellular matrix in symptomatic women. *Semin Reprod Med* 2010;**28**: 169–179.

Mas A, Cervello I, Gil-Sanchis C, Faus A, Ferro J, Pellicer A, Simon C. Identification and characterization of the human leiomyoma side population as putative tumor-initiating cells. *Fertil Steril* 2012;**98**:741–751 e746.

Mas A, Nair S, Laknaur A, Simon C, Diamond MP, Al-Hendy A. Stro-1/CD44 as putative human myometrial and fibroid stem cell markers. *Fertil Steril* 2015;**104**:225–234 e223.

Masuda H, Anwar SS, Buhring HJ, Rao JR, Gargett CE. A novel marker of human endometrial mesenchymal stem-like cells. *Cell Transplant* 2012;**21**:2201–2214.

Mercorio F, De R, Di A, Cerrota G, Bifulco G, Vanacore F, Nappi C. The effect of a levonorgestrel-releasing intrauterine device in the treatment of myoma-related menorrhagia. *Contraception* 2003;**67**:277–280.

Mukherjee A, Patterson AL, George JW, Carpenter TJ, Madaj ZB, Hostetter G, Risinger JI, Teixeira JM. Nuclear PTEN localization contributes to DNA damage response in endometrial adenocarcinoma and could have a diagnostic benefit for therapeutic management of the disease. *Mol Cancer Ther* 2018.

Noe M, Kunz G, Herbertz M, Mall G, Leyendecker G. The cyclic pattern of the immunocytochemical expression of oestrogen and progesterone receptors in human myometrial and endometrial layers: characterization of the endometrial-subendometrial unit. *Hum Reprod* 1999;**14**:190–197.

Olson MR, Su R, Flaws JA, Fazleabas AT. Bisphenol A impairs decidualization of human uterine stromal fibroblasts. *Reprod Toxicol* 2017;**73**:339–344.

Ono M, Bulun SE, Maruyama T. Tissue-specific stem cells in the myometrium and tumor-initiating cells in leiomyoma. *Biol Reprod* 2014;**91**:149.

Ono M, Kajitani T, Uchida H, Arase T, Oda H, Uchida S, Ota K, Nagashima T, Masuda H, Miyazaki K *et al.* CD34 and CD49f double-positive and lineage marker-negative cells isolated from human myometrium exhibit stem cell-like properties involved in pregnancy-induced uterine remodeling. *Biol Reprod* 2015;**93**:37.

Ono M, Maruyama T, Masuda H, Kajitani T, Nagashima T, Arase T, Ito M, Ohta K, Uchida H, Asada H *et al.* Side population in human uterine myometrium displays phenotypic and functional characteristics of myometrial stem cells. *Proc Natl Acad Sci U S A* 2007;**104**:18700–18705.

Ono M, Qiang W, Serna VA, Yin P, JSt C, Navarro A, Monsivais D, Kakinuma T, Dyson M, Druschitz S *et al.* Role of stem cells in human uterine leiomyoma growth. *PLoS One* 2012;**7**:e36935.

Qureshi-Baig K, Ullmann P, Haan S, Letellier E. Tumor-initiating cells: a criTICal review of isolation approaches and new challenges in targeting strategies. *Mol Cancer* 2017;**16**:40.

Roeder BA, Kokini K, Sturgis JE, Robinson JP, Voytik-Harbin SL. Tensile mechanical properties of three-dimensional type I collagen extracellular matrices with varied microstructure. *J Biomech Eng* 2002;**124**:214–222.

Schwab KE, Gargett CE. Co-expression of two perivascular cell markers isolates mesenchymal stem-like cells from human endometrium. *Hum Reprod* 2007;**22**:2903–2911.

Sivasubramaniyan K, Harichandan A, Schumann S, Sobiesiak M, Lengerke C, Maurer A, Kalbacher H, Buhring HJ. Prospective isolation of mesenchymal stem cells from human bone marrow using novel antibodies directed against sushi domain containing 2. *Stem Cells Dev* 2013;**22**:1944–1954.

Smithson M, Verkuilen J. A better lemon squeezer? Maximum-likelihood regression with beta-distributed dependent variables. *Psychol Methods* 2006;**11**:54–71.

Szotek PP, Chang HL, Zhang L, Preffer F, Dombkowski D, Donahoe PK, Teixeira J. Adult mouse myometrial label-retaining cells divide in response to gonadotropin stimulation. *Stem Cells* 2007;**25**:1317–1325.

Team, R Core. 2018. 'R: A language and environment for statistical computing'.

Teixeira J, Rueda BR, Pru JK. Uterine stem cells. In: *StemBook*. Cambridge (MA), 2008, doi/10.3824/stembook.1.16.1, https://www.stembook.org

Valenti MT, Dalle Carbonare L, Mottes M. Osteogenic differentiation in healthy and pathological conditions. *Int J Mol Sci* 2016;**18**.

Vemuri MC, Chase LG, Rao MS. Mesenchymal stem cell assays and applications. *Methods Mol Biol* 2011;**698**:3–8.

Walker CL, Stewart EA. Uterine fibroids: the elephant in the room. *Science* 2005;**308**:1589–1592.

Wong SP, Rowley JE, Redpath AN, Tilman JD, Fellous TG, Johnson JR. Pericytes, mesenchymal stem cells and their contributions to tissue repair. *Pharmacol Ther* 2015;**151**:107–120.

Wu JM, Wechter ME, Geller EJ, Nguyen TV, Visco AG. Hysterectomy rates in the United States, 2003. *Obstet Gynecol* 2007;**110**:1091–1095.

Yin P, Ono M, Moravek MB, JSt C, Navarro A, Monsivais D, Dyson MT, Druschitz SA, Malpani SS, Serna VA *et al.* Human uterine leiomyoma stem/progenitor cells expressing CD34 and CD49b initiate tumors in vivo. *J Clin Endocrinol Metab* 2015;**100**:E601–E606.

Zhang P, Zhang C, Hao J, Sung CJ, Quddus MR, Steinhoff MM, Lawrence WD. Use of X-chromosome inactivation pattern to determine the clonal origins of uterine leiomyoma and leiomyosarcoma. *Hum Pathol* 2006;**37**:1350–1356.

Zhou BB, Zhang H, Damelin M, Geles KG, Grindley JC, Dirks PB. Tumour-initiating cells: challenges and opportunities for anticancer drug discovery. *Nat Rev Drug Discov* 2009;**8**:806–823.